New and Existing Techniques for Dynamic Loads Analyses of Flexible Airplanes

Anthony S. Pototzky*
PRC—Kentron, Inc., Hampton, Virginia
and
Boyd Perry III†
NASA Langley Research Center, Hampton, Virginia

This paper reviews existing techniques for calculating dynamic loads for flexible airplanes and presents a new technique. The new technique involves the summation-of-forces method of writing dynamic loads equations. Until now, this form of the dynamic loads equations has been formulated in the frequency domain. The new technique uses *s*-plane approximation methods (previously applied only to the equations of motion) to transform the dynamic loads equations from a second-order frequency domain formulation with frequency-dependent coefficients into a linear-time-invariant state-space formulation. Several numerical examples demonstrate the usefulness of the new technique and the high quality of the results. In addition, a convergence investigation establishes that the summation-of-forces method converges more quickly (that is, with fewer modes) than does the mode displacement method.

Nomenclature

$A_0, A_1, \ldots, A_6$ = approximating coefficient matrices for generalized aerodynamic forces
$\bar{A}_0, \bar{A}_1, \ldots, \bar{A}_6$ = approximating coefficient matrices for aerodynamic component of SFM dynamic loads
b = reference semichord
C = matrix of MDM load coefficients
D = generalized damping matrix
$\tilde{D}$ = augmented structural damping matrix
$\bar{D}$ = SFM dynamic load matrix due to aerodynamic damping
f_{ij} = force applied at location i for flexible mode j (see Fig. 1)
I = identity matrix
i = $\sqrt{-1}$
K = generalized stiffness matrix
$\tilde{K}$ = augmented structural stiffness matrix
$\bar{K}$ = SFM dynamic load matrix due to aerodynamic stiffness
k = reduced frequency, $\omega b/v$
L = vector of dynamic loads
M = generalized mass matrix
$\bar{M}$ = inertial matrix in SFM dynamic load equations
$\tilde{M}$ = augmented structural mass matrix
$\bar{M}$ = augmented inertial matrix in SFM dynamic load equations
Q, Q_c, Q_G = generalized aerodynamic force coefficient matrices due to motion, control deflection, and gust
$\bar{Q}, \bar{Q}_c, \bar{Q}_G$ = SFM dynamic load matrices due to motion, control deflection, and gust aerodynamics
q, q_c = vectors of generalized coordinates and control deflections
$\bar{q}$ = dynamic pressure, $\frac{1}{2}\rho v^2$
s = Laplace variable
t = time
u_c, u_G = vectors of control and gust inputs; $u_c = q_c$; $u_G = w_g$
v = freestream velocity
w_g = vertical gust velocity
x_1 = state vector representing q
x_2 = state vector representing $\dot{q}$
x_3, x_4, x_5, x_6 = state vectors representing aerodynamic lags
y_i = moment arm (see Fig. 1)
z_{ij} = vertical displacement at location i for flexible mode j (see Fig. 1)
β_i = aerodynamic lag
$\bar{\beta}_i$ = $(v/b)\beta_i$
ρ = fluid density
σ = root mean square value
$\Phi(\omega)$ = power spectral density function
ω = circular frequency
$\dot{(\ )}$ = time derivative

Received March 14, 1985; presented as Paper 85-0808 at the AIAA/ASME/ASCE/AHS 26th Structures, Structural Dynamics and Materials Conference, Orlando, FL, April 15-17, 1985; revision received Oct. 17. 1985. This paper is declared a work of the U.S. Government and is not subject to copyright protection in the United States.

*Engineering Specialist, Aerospace Technologies Division. Member AIAA.

†Aerospace Engineer, Aeroservoelasticity Branch, Loads and Aeroelasticity Division. Member AIAA.

Introduction

HISTORICALLY, the equations of motion (EOM) and the dynamic loads equations (DLE) of flexible airplanes have been formulated in the frequency domain with the unsteady aerodynamic forces being transcendental functions of frequency. Within the past decade, however, it has become common practice to employ so-called "*s*-plane approximation" techniques to the aerodynamic coefficients within the EOM.[1,2] These techniques convert the original tabular nature of the frequency dependency of each aerodynamic coefficient to an approximating rational polynomial in the Laplace variable s. With this technique employed, the EOM may then be transformed into a linear-time-invariant (LTI) state-space formulation. This formulation makes available a wide range of computational tools for performing multivariable control system analysis and synthesis tasks. A significant number of papers already published (e.g., Refs. 1-10) attest to the computational advantage of casting flexible-airplane equations in the state-space formulation.

Currently, the two most common methods of calculating incremental airplane loads are the mode displacement method (MDM) and the summation-of-forces method (SFM). These two and a third method, the mode acceleration method (MAM), are described in Ref. 11. All give theoretically identical answers for a sufficient number of modes. Reference 11 illustrates, by example, that the MAM "shows a superiority in convergence over" the MDM. However, Ref. 11 does not offer a comparison of the convergence characteristics of the MDM and the SFM. One of the purposes of this paper is to present such a comparison.

A major difference between the MDM and the SFM is that the DLE obtained using the SFM contain frequency-dependent aerodynamic coefficients, while DLE obtained using the MDM do not. Because of this frequency dependency, to date the SFM has been restricted to analyses performed with transcendental frequency domain EOM. The MDM, on the other hand, is applicable in either the transcendental frequency domain or the LTI state-space representation. The second, and major, purpose of this paper is to present the conversion of the frequency-dependent SFM coefficients to approximating rational polynomials in the Laplace variable and, then, present the transformation of the resulting DLE into an LTI state-space representation. Several numerical examples are presented.

Terminology

This paper deals with equations of motion (EOM) and dynamic loads equations (DLE) in either a transcendental frequency domain formulation or an LTI state-space formulation. The DLE may be obtained by either the summation-of-forces method (SFM) or mode displacement method (MDM). For brevity, the term "formulation" will refer to either the transcendental frequency domain representation of the EOM and DLE or the LTI state-space representation of the EOM and DLE; the term "method" will refer to either the SFM or the MDM. As indicated in Table 1, there are four possible combinations of formulation and method.

The term "technique" will always refer to one of these possible combinations. Recalling the title of this paper, the new and existing techniques are indicated in Table 1.

Equations of Motion

The following discussion of the equations of motion for a flexible airplane serves as background information for subsequent discussions of the dynamic load equations.

Development of Transcendental Frequency Domain Formulation of EOM

The equations of motion are derived through a modal approach using Lagrange's equations. The resulting equations are linearized small-perturbation equations about a particular (usually trimmed 1 g) operating point. These equations are expressed in matrix form in the Laplace domain as,

$$\left(s^2[M{:}M_c]+s[D{:}0]+[K{:}0]\right)\left\{\frac{q(s)}{q_c(s)}\right\}+\frac{1}{2}\rho v^2[Q(s){:}Q_c(s)]\left\{\frac{q(s)}{q_c(s)}\right\}+\frac{1}{2}\rho v^2\{Q_G(s)\}\frac{w_g}{v}=\{0\} \tag{1}$$

where $q(s)$ and $q_c(s)$ are the vectors of generalized coordinates and control surface deflections, respectively. For simplicity, aerodynamic hinge moments and hinge moments due to inertial coupling between the control surface and other modes have been neglected in Eq. (1). Equation (1) is solved for $q(s)$. The elements of $[M]$, $[M_c]$, $[D]$, and $[K]$ are real constants and are obtained from finite element structural analysis codes, such as Refs. 12 and 13. The elements of $[Q(s)]$, $[Q_c(s)]$, and $[Q_G(s)]$ are complex transcendental functions of the Laplace variable s. In actual practice, the unsteady aerodynamic forces are typically computed for oscillatory motion using finite element panel method codes, such as Refs. 14 and 15. For this reason, engineers have, for many years, implemented and solved Eq. (1) (for performing flutter and gust analyses, for example) in the frequency domain. Rewriting Eq. (1) in the frequency domain yields

$$\left(-\omega^2[M{:}M_c]+i\omega[D{:}0]+[K{:}0]\right)\left\{\frac{q(i\omega)}{q_c(i\omega)}\right\}+\frac{1}{2}\rho v^2[Q(ik){:}Q_c(ik)]\left\{\frac{q(i\omega)}{q_c(i\omega)}\right\}+\frac{1}{2}\rho v^2\{Q_G(ik)\}\frac{w_g}{v}=\{0\} \tag{2}$$

s-Plane Approximation Applied to EOM

As mentioned earlier, it has become common practice to employ so-called "s-plane approximation" techniques to the aerodynamic coefficients within Eq. (1). These techniques convert the original tabular nature of the frequency dependency of each coefficient to an approximating rational polynomial in the Laplace variable s. The s-plane approximation is applied to all elements of $[Q(s){:}Q_c(s)]$ and $\{Q_G(s)\}$. A typical element is represented by

$$Q(s)\doteq A_0+A_1\left(\frac{b}{v}\right)s+A_2\left(\frac{b}{v}\right)^2s^2+\sum_{m=3}^{6}\frac{A_m s}{[s+(v/b)\beta_{m-2}]} \tag{3}$$

As described in Ref. 4, the form of Eq. (3) permits an approximation of the time delays inherent in unsteady aerodynamics subject to the following requirements: real approximating coefficients, denominator roots in the left-hand plane, and a good approximation of the complex aerodynamic terms at $s=i\omega$. The approximating coefficients $(A_0,A_1,\ldots,A_6)$ in Eq. (3) are evaluated by a least-squares curve fit[4,5] given the values of complex aerodynamic terms at a number of discrete values of reduced frequency. The values

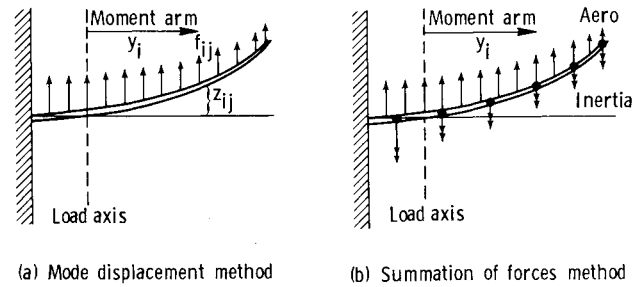

(a) Mode displacement method (b) Summation of forces method

Fig. 1 Forces comprising two dynamic loads methods.

Table 1 Combinations of formulation and method

Method of obtaining DLE	Formulation of EOM and DLE: Transcendental frequency domain	Formulation of EOM and DLE: LTI state-space
SFM	Existing	New
MDM	Existing	Existing

of β_1, β_2, β_3, and β_4 from the denominator of Eq. (3) are arbitrary, but they are usually set to values within the range of reduced frequencies.

LTI State-Space Formulation of EOM

Once the equations of motion exist with the s-plane approximation incorporated into the equations, it is a routine step to then transform them into the following LTI state-space formulation in the time domain,[10]

$$\begin{Bmatrix} \dot{x}_1 \\ \dot{x}_2 \\ \dot{x}_3 \\ \vdots \\ \dot{x}_6 \end{Bmatrix} = \begin{bmatrix} & 0 & [I] & 0 & 0 \\ -\tilde{M}^{-1} & (\tilde{K} & \tilde{D} & \tilde{q}[\mathrm{I}] & \tilde{q}[I]) \\ & 0 & A_3 & -\tilde{\beta}_1[I] & 0 \\ & \vdots & \vdots & \vdots & \\ & 0 & A_6 & 0 & -\tilde{\beta}_4[I] \end{bmatrix} \begin{Bmatrix} x_1 \\ x_2 \\ x_3 \\ \vdots \\ x_6 \end{Bmatrix}$$

$$+ \begin{bmatrix} & 0 & 0 & 0 \\ -\tilde{M}^{-1} & (\tilde{K}_c & \tilde{D}_c & \tilde{M}_c) \\ & 0 & A_{c_3} & 0 \\ & \vdots & \vdots & \vdots \\ & 0 & A_{c_6} & 0 \end{bmatrix} \begin{Bmatrix} u_c \\ \dot{u}_c \\ \ddot{u}_c \end{Bmatrix}$$

$$+ \begin{bmatrix} & 0 & 0 & 0 \\ -\tilde{M}^{-1} & (\tilde{K}_G & \tilde{D}_G & \tilde{M}_G) \\ & 0 & A_{G_3} & 0 \\ & \vdots & \vdots & \vdots \\ & 0 & A_{G_6} & 0 \end{bmatrix} \begin{Bmatrix} u_G \\ \dot{u}_G \\ \ddot{u}_G \end{Bmatrix} \tag{4}$$

where

$$\tilde{M} = M + \tilde{q}(b/v)^2 A_2, \quad \tilde{D} = D + \tilde{q}(b/v) A_1, \quad \tilde{K} = K + \tilde{q} A_0$$

This state-space formulation makes available a wide range of computational tools for performing multivariable control system analysis and synthesis tasks. The x_1 state vector above is the generalized coordinate vector q in Eq. (1). The x_2 vector is the time derivative of x_1. Vectors x_2-x_6 are aerodynamic lag states. The submatrices in the system matrix are composed of M, D, and K matrices from Eq. (1) and parts of the $Q(s)$ matrix in Eq. (3). The input effectiveness matrices are presented in a general fashion for gust and control surface inputs. Vectors u_c and u_G are the control surface and gust input vectors, respectively.

Dynamic Loads Equations—Existing Techniques

The two most common methods of calculating incremental airplane loads are the mode displacement method (MDM) and the summation-of-forces method (SFM). Both methods require the solution of the equations of motion (i.e., the vector of generalized coordinates—and, in the case of SFM, the second derivative of this vector) and both give theoretically identical answers for a sufficient number of modes. Brief developments of the MDM and the SFM follow.

Mode Displacement Method (MDM)

The MDM is based on the internal forces of the elastic structure. For each load (shears, bending moments, and torsional moments at several locations on the vehicle), load coefficients are obtained for each elastic mode. (Load coefficients for rigid-body and rigid-control-surface modes are zero.) The following discussion outlines the manner in which the load coefficients are obtained for a single elastic mode at one load station. The extension to other elastic modes and other load stations is obvious.

Figure 1a is a front view of a wing deflected into the mode shape of one of its elastic modes. The arrows indicate the forces (applied normal to the wing surface at structural nodes) required to produce this deflected shape. With the magnitude of each force known through the stiffness matrix, shears, bending moments, and torsional moments (at any location) due to these forces may be computed. The sum of all forces outboard of the load station is the shear; the sum of the products of all forces outboard of the load station times their appropriate moment arms are the moments. Such shears and moments are, then, the load coefficients for this particular elastic mode. Load coefficients for the remaining elastic modes can be found in an identical manner.

Transcendental Frequency-Domain Formulation

The transcendental frequency domain formulation of the DLE for the MDM is given by

$$\{L(i\omega)\} = [C]\{q(i\omega)\} \tag{5}$$

where $\{L(i\omega)\}$ is the vector of dynamic loads; $[C]$ is the matrix of load coefficients; and $q(i\omega)$, the vector of generalized coordinates, is the solution of Eq. (2). Each element of matrix $[C]$ is a real constant.

LTI State-Space Formulation

The LTI state-space formulation of the DLE for the MDM is analogous to Eq. (5) and is given by

$$\{L(t)\} = [C\ 0\ 0\ \ldots\ 0] \begin{Bmatrix} x_1 \\ x_2 \\ x_3 \\ \vdots \\ x_6 \end{Bmatrix} \tag{6}$$

where here submatrix C is identical to $[C]$ in Eq. (5) and the state vector is the solution to Eq. (4).

Summation-of-Forces Method (SFM)

In the SFM, shears, bending moments, and torsional moments are obtained by summing inertial forces and moments as well as forces and moments resulting from unsteady aerodynamic pressures on the vehicle. The aerodynamic forces and moments are further broken down into those due to vehicle motion and those due to disturbance.

Figure 1b illustrates the inertia and aerodynamic components of the loads for finite element representations of the vehicle. Aerodynamic forces are depicted as single-headed arrows. Inertia forces are depicted as double-headed arrows. Using the results from an unsteady aerodynamic panel method, the magnitude of each single-headed arrow is equal to the product of the unsteady pressure acting on a panel times the area of that panel. The magnitude of each double-headed arrow is equal to the product of a lumped mass (obtained from a structural analysis code) times the acceleration of that mass.

Consistent with the EOM expressed in Eq. (1), the general form of the SFM load equations is

$$\{L(s)\} = s^2 [\bar{M}:\bar{M}_c] \begin{Bmatrix} q(s) \\ q_c(s) \end{Bmatrix}$$

$$+ \frac{1}{2} \rho v^2 [\bar{Q}(s):\bar{Q}_c(s)] \begin{Bmatrix} q(s) \\ q_c(s) \end{Bmatrix}$$

$$+ \frac{1}{2} \rho v^2 \{\bar{Q}_G(s)\} \frac{w_g}{v} \tag{7}$$

where $L(s)$ is a vector of dynamic loads. The first term on the right side of the equation represents inertia forces, the second term aerodynamic forces due to vehicle motion and control surface deflection, and the third term aerodynamic forces due to gust disturbances. The elements of $[\bar{M}]$ and $[\bar{M}_c]$ are real constants. The elements of $[\bar{Q}(s):\bar{Q}_c(s)]$ and $\{\bar{Q}_G(s)\}$ are complex and transcendental functions of s.

Transcendental Frequency-Domain Formulation

The transcendental frequency domain formulation of the DLE for the SFM is obtained by rewriting Eq. (7) in the form

$$\{L(i\omega)\} = -\omega^2[\bar{M}:\bar{M}_c]\left\{\frac{q(i\omega)}{q_c(i\omega)}\right\} + \frac{1}{2}\rho v^2[\bar{Q}(ik):\bar{Q}_c(ik)]\left\{\frac{q(i\omega)}{q_c(i\omega)}\right\} + \frac{1}{2}\rho v^2\{\bar{Q}_G(ik)\}\frac{w_g}{v} \tag{8}$$

where $q(i\omega)$ is the solution of Eq. (2).

Dynamic Loads Equations—New Technique

The new technique is the LTI state-space formulation of the DLE for the SFM. The development parallels that in the section on the equations of motion.

s-Plane Approximation Applied to SFM

The frequency-dependent aerodynamic load coefficients within Eq. (8) can be represented by rational polynomial functions in exactly the same form as those used in the EOM because the elements of $[\bar{Q}(ik):\bar{Q}_c(ik)]$ an $\{\bar{Q}_G(ik)\}$ are constructed in a manner similar to the elements of $[Q(ik):Q_c(ik)]$ and $\{Q_G(ik)\}$. The s-plane approximation for a typical element of $[\bar{Q}(s):\bar{Q}_c(s)]$ or $\{\bar{Q}_G(s)\}$ is represented by

$$\bar{Q}(s) \doteq \bar{A}_0 + \bar{A}_1\left(\frac{b}{v}\right)s + \bar{A}_2\left(\frac{b}{v}\right)^2 s^2 + \sum_{m=3}^{6}\frac{\bar{A}_m s}{(s+(v/b)\beta_{m-2})} \tag{9}$$

As in Eq. (3), the approximating coefficients $(\bar{A}_0,\bar{A}_1,\ldots,\bar{A}_6)$ in Eq. (9) are obtained by a least-squares curve fit. A typical curve fit (in this case, first bending mode contribution to wing root bending moment) employing Eq. (9) is presented in Fig. 2.

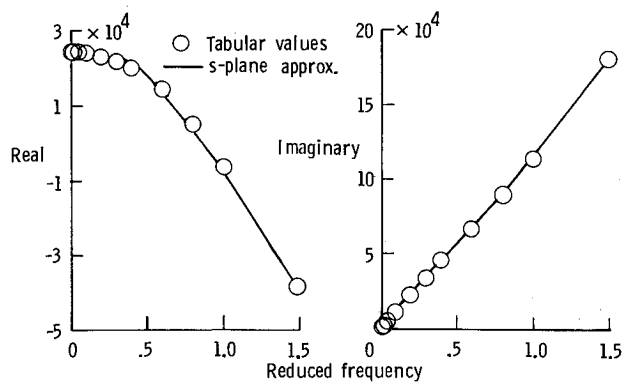

Fig. 2 Aerodynamic load coefficient due to airplane motion.

LTI State-Space Formulation of SFM

For simplicity, in this section of the paper, the "LTI state-space SFM dynamic load equations" will be referred to as the "output equation." Formulation of the output equation can be accomplished many possible ways, but the particular form of the output equation used in this paper is consistent with the EOM expressed in Eq. (4). Equation (4) is the form of the EOM coded in two of the computer programs (ISAC and KONPACT) used in the implementation of the new technique (see the next section). Most of the terms of the following output equation can be obtained with little difficulty by substituting Eq. (9) into Eq. (8) and then associating the resulting submatrices with the appropriate state vectors of Eq. (4). The remaining terms involve some matrix operations in which the "lag" states are internally transformed into the generalized coordinates.

$$\{L(t)\} = \begin{bmatrix} \tilde{M}\bar{M}^{-1}(\bar{K}\ \bar{D}\ \bar{q}I & \ldots\bar{q}I) \\ \tilde{\bar{K}}\ \tilde{\bar{D}}\ \bar{q}\bar{A}_3A_3^{-1}\ldots\bar{q}\bar{A}_6A_6^{-1} & \end{bmatrix}\begin{Bmatrix} x_1 \\ x_2 \\ x_3 \\ \vdots \\ x_6 \end{Bmatrix} + \begin{bmatrix} \tilde{M}\bar{M}^{-1}(\bar{K}_c & \bar{D}_c & \bar{M}_c) \\ \tilde{\bar{K}}_c\ \tilde{\bar{D}}_c + \bar{q}\sum_{i=1}^{4}(\bar{A}_{ci+2} - \bar{A}_{i+2}A_{i+2}^{-1}A_{ci+2})\tilde{\bar{M}}_c & & \end{bmatrix}\begin{Bmatrix} u_c \\ \dot{u}_c \\ \ddot{u}_c \end{Bmatrix} + \begin{bmatrix} \tilde{M}\bar{M}^{-1}(\bar{K}_G & \bar{D}_G & \bar{M}_G) \\ \tilde{\bar{K}}_G\ \tilde{\bar{D}}_G + \bar{q}\sum_{i=1}^{4}(\bar{A}_{Gi+2} - \bar{A}_{i+2}A_{i+2}^{-1}A_{Gi+2})\tilde{\bar{M}}_G & & \end{bmatrix}\begin{Bmatrix} u_G \\ \dot{u}_G \\ \ddot{u}_G \end{Bmatrix} \tag{10}$$

where

$$\tilde{\bar{M}} = \bar{M} + \bar{q}\left(\frac{b}{v}\right)^2\bar{A}_2, \quad \tilde{\bar{D}} = \bar{q}\left(\frac{b}{v}\right)\bar{A}_1, \quad \tilde{\bar{K}} = \bar{q}\bar{A}_0$$

The first row of submatrices in Eq. (10) represents the inertia component of the loads; the second row represents the aerodynamic component.

Implementation of New Technique

This section deals with the computer implementation of the new technique. Figure 3 is a flow chart illustrating the relationships and flow of information between the systems of

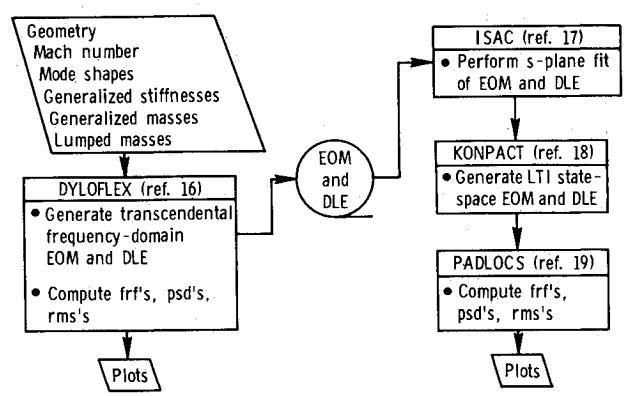

Fig. 3 Implementation of new technique.

computer programs used in this implementation. The name and function of each system of programs is indicated in the figure. There are a significant number of omissions of additional (and, in some cases, duplicated) capabilities of these systems of programs. With these omissions in mind, the left side of the figure represents the transcendental frequency domain formulation of the EOM and DLE; the right side represents the LTI state-space formulation.

Transcendental Frequency Domain Formulation of EOM and DLE

The primary inputs required are indicated in the top left corner of Fig. 3. The DYLOFLEX[16] system of programs is used here to formulate and solve the EOM and the SFM DLE in the frequency domain. The EOM as expressed in Eq. (2) and the DLE as expressed in Eqs. (5) and (8) are solved in DYLOFLEX, producing, as final answers, frequency response functions (FRFs), power spectral density (PSD) functions, root mean square (rms) values, and associated plots.

LTI State-Space Formulation of EOM and DLE

The transcendental frequency domain formulation of EOM and DLE (as created by DYLOFLEX) are written on a magnetic file, as indicated in Fig. 3, and serve as the starting point for the LTI state-space formulation. This file is read by the ISAC[17] system of programs, which performs s-plane fits of the EOM and SFM DLE according to Eqs. (3) and (9). Next, the KONPACT[18] system of programs takes these s-plane fits and other necessary information and creates state-space EOM and SFM DLE according to Eqs. (4) and (10). Finally, the PADLOCS[19] system of programs takes the LTI state-space form of the equations and solves them, producing FRFs, PSD functions, rms values, and plots.

Numerical Examples

This section of the paper presents, first, a comparison of the convergence characteristics of the MDM and SFM and, second, two applications of the new technique. The configuration chosen for all results presented in this section is the NASA DAST ARW-2 airplane. In the NASA DAST (Drones and Aerodynamics and Structural Testing) Project, Firebee II target drones are modified by the removal of the standard wing and the installation of aeroelastic research wings (ARW). The second research wing in the series, ARW-2, has a supercritical airfoil, high aspect ratio (10.3), and low sweep angle (25 deg for the half-chord line). The reference semichord is 11.74 in. A sketch of the NASA DAST ARW-2 airplane is shown in Fig. 4.

The convergence investigation and first application use the right semispan of ARW-2 as a cantilevered wind tunnel model. (No test results are presented.) Mode shapes, generalized masses, and generalized stiffnesses for the first eight flexible modes, as well as the lumped masses, were obtained from a structural analysis program. The disturbance quantity in the equations of motion and dynamic load equations is the sinusoidal deflection of an outboard control surface on the wing. A doublet lattice code was used to generate unsteady pressures. The corresponding aerodynamic box layout is shown in Fig. 5. The circle symbols represent the points at which the dynamic load (shear, bending moment, torsional moment) frequency response functions were calculated. The analysis for this configuration were performed at a Mach number of 0.7 and at a dynamic pressure of 100 lb/ft^2. The freestream velocity for this condition is 4242 in./s.

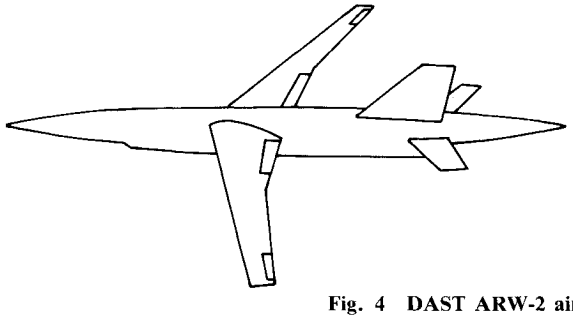

Fig. 4 DAST ARW-2 aircraft.

Convergence Investigation: Comparison of SFM and MDM

The purpose of this comparison is to determine which method, the SFM or the MDM, converges more quickly to the theoretical answer. Figure 6 presents frequency response functions of wing root bending moment (WRBM) for both methods calculated by use of the LTI state-space formulation. All eight flexible modes are present in each method. The magnitudes are in very close agreement over the entire frequency range. With the exception of the disagreement in the vicinity of 300 rad/s, the same is true for the phase angles. This comparison is typical of the very good agreement between methods for all load stations and for all loads

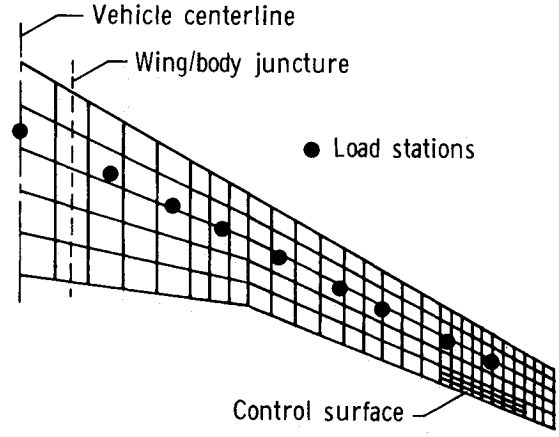

Fig. 5 Aerodynamic box layout for ARW-2 right semispan.

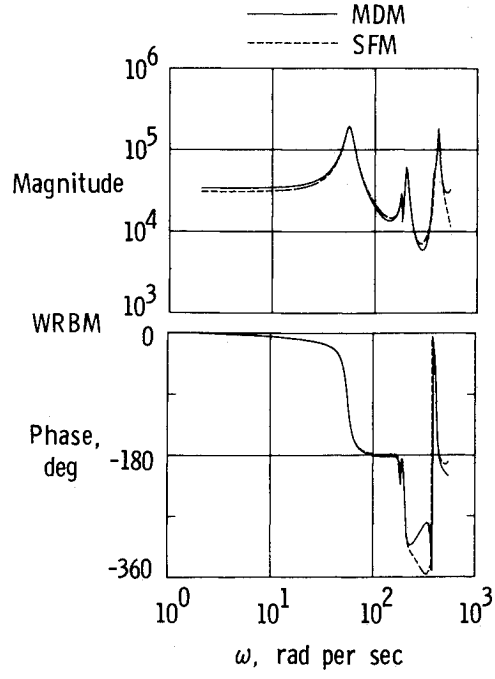

Fig. 6 Comparison of MDM and SFM wing root bending moment frequency response functions due to control surface deflection.

and confirms that, with a sufficient number of modes, SFM and MDM converge to the same answer.

Figure 7 illustrates the effects on the load frequency response functions of truncating flexible modes. The wing root torsional moment (WRTM) is presented in this figure because it experienced the most pronounced effects. The solid lines are results obtained by retaining all eight flexible modes in the analysis; the dashed lines are results obtained by retaining only the first three flexible modes. Figure 7a contains the MDM results, Fig. 7b, the SFM results. It is obvious from Fig. 7a that, in truncating five flexible modes from the MDM analysis, both the magnitude and phase angle changed significantly over the entire frequency range. This is not the case in Fig. 7b. There is very good agreement for the SFM analysis up to about 200 rad/s (the natural frequency of the third flexible mode).

Significant disagreement between three-modes-retained and 8-modes-retained analyses occurs only at frequencies higher than the natural frequency of highest retained mode. Therefore, the SFM converges more quickly than ("shows a superiority of convergence over") the MDM.

Application of New Technique: Frequency Response due to Control Deflection

Figure 8 shows the wing root bending moment frequency response functions. The dashed curves were obtained from the SFM transcendental frequency domain analysis and the solid curve from the new SFM LTI state-space analysis. There is excellent agreement between the magnitudes (they are almost coincident) over the entire frequency range and there is very good agreement between the phase angles. Although not shown, the agreement between transcendental and state-space results for all other loads at all load stations was as good as or better than that shown in Fig. 8.

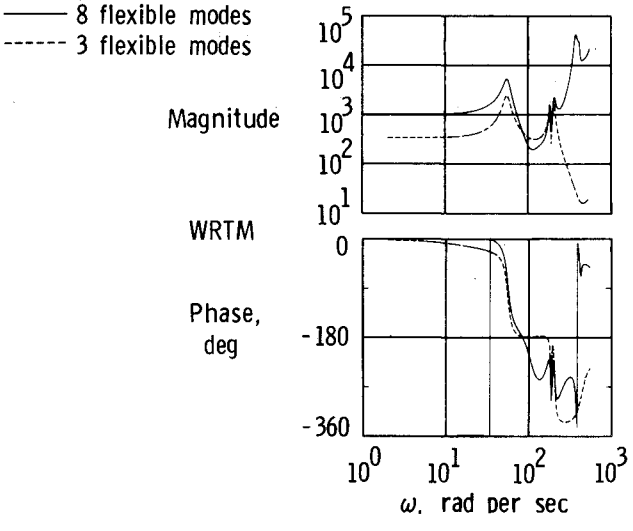

a) Mode displacement method.

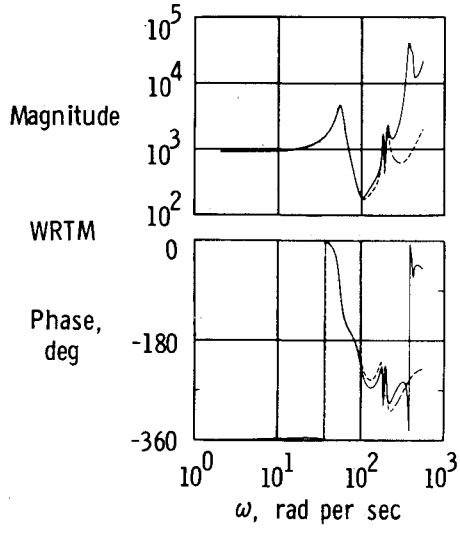

b) Summation-of-forces method.

Fig. 7 Effect of truncating flexible modes on wing root torsional moment frequency response functions due to control surface deflection.

Application of New Technique: Gust Load Analysis

The configuration chosen for the second application is the complete DAST ARW-2 airplane. Gust loads were calculated for ARW-2 at analysis conditions corresponding to flight at a Mach number of 0.7 and an altitude of 15,000 ft. The freestream velocity for this condition is 8877 in./s. In the analysis, two rigid-body modes (plunge and pitch) and the first eight flexible modes were included. The aerodynamic box layout for this configuration is shown in Fig. 9. The circles represent the locations at which shear, bending moment, and torsional moment were calculated.

In the present example, transcendental/state-space comparisons are made of load FRFs, load PSD functions, and load rms values due to gusts. The Dryden form of the one-dimensional gust PSD function (with gust length of 2500 ft) was chosen for these comparisons.

Figure 10 contains a comparison of wing-root bending moment FRFs due to gust. Magnitude and phase plots are presented. The solid curve is from the state-space analysis and the dashed curve from the transcendental analysis. There is excellent agreement for the magnitudes over almost the entire frequency range (2-500 rad/s). The comparison of phase angles shows some discrepancies over the frequency range, but is still considered to be very good. Figure 11 contains comparisons of PSD functions of the wing root bending and torsional moments. Again, there is excellent agreement for each over almost the entire frequency range.

Figure 12 contains comparisons of load rms values as a function of semispan. The solid curves are from the state-space analysis and the dashed curves from the transcendental analysis. Considering the high quality of the comparisons shown in Figs. 10 and 11 for the wing root, it is not surprising that this trend continues out the span. The largest differences in rms values occur at the tip, but, because of the scale of the figure, are too small to be seen. The differences

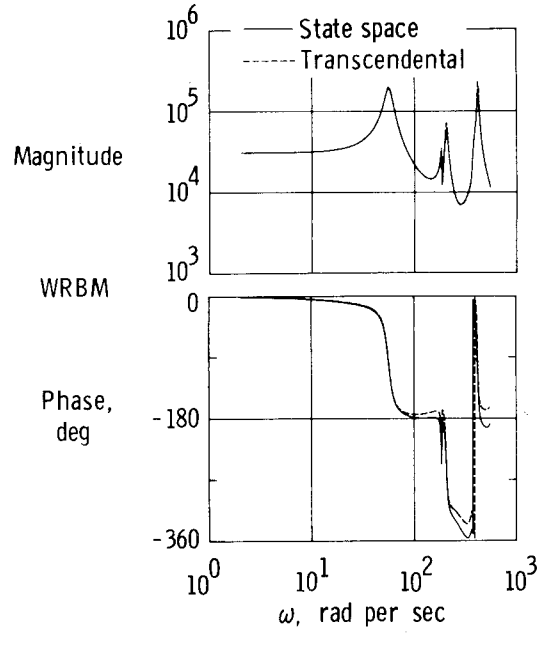

Fig. 8 Comparison of transcendental and state-space wing root bending moment frequency response functions due to control surface deflection.

Table 2 Comparison of dynamic loads method

Mode displacement method +/−	Attribute	Summation-of-forces method +/−	Attribute
+	Load coefficients available without need for unsteady aerodynamics	−	Load coefficients available only after unsteady aerodynamics obtained
+	Load coefficients are real and frequency independent (trivial bookkeeping effort)	−	Load coefficients are complex and frequency dependent (sizable bookkeeping effort)
+	Dynamic load equations can be easily cast in state-space form	+	Dynamic load equations can be cast in state-space form
−	Can compute only the total load acting on the vehicle	+	Can selectively compute components (aerodynamic or inertia) of the total load acting on the vehicle
−	Slower convergence with increasing number of retained modes	+	Faster convergence with increasing number of retained modes

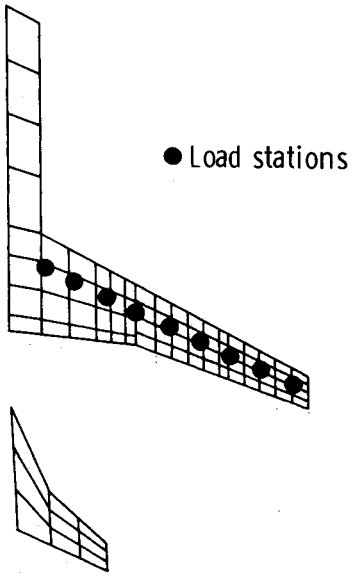

Fig. 9 Aerodynamic box layout for DAST ARW-2.

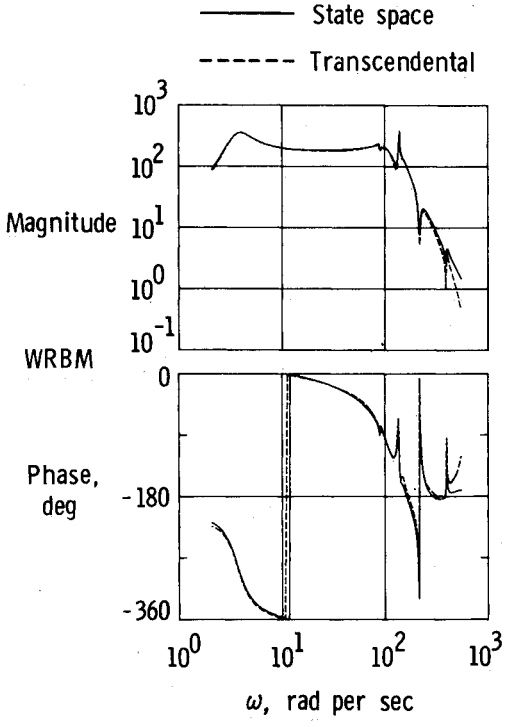

Fig. 10 Comparison of transcendental and state-space wing root bending moment frequency response functions due to gust.

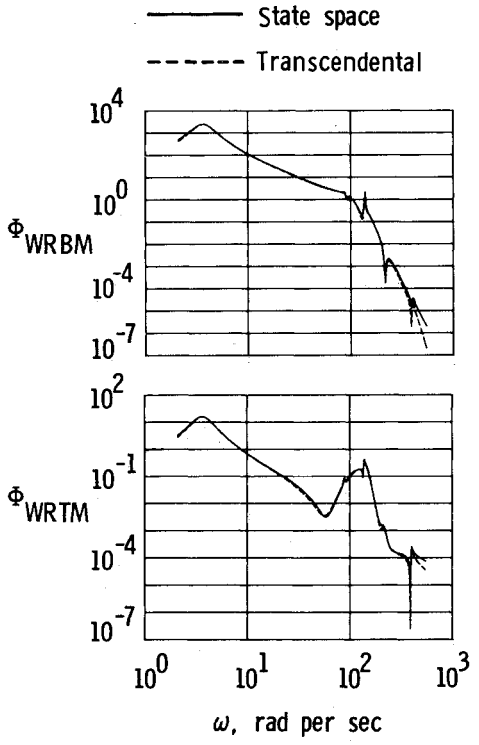

Fig. 11 Comparison of transcendental and state-space dynamic load power spectral density functions.

at the tip are 2.1% for shear, 4.1% for bending moment, and 3.5% for torsional moment.

Discussion

These two applications of the new technique illustrate that the technique works. However, it should be emphasized at this point that the quality of the answers obtained with the new technique is strongly dependent on the quality of the *s*-plane approximations of both the generalized aerodynamic forces and the SFM aerodynamic matrices. Good approximations will provide good results; bad approximations, bad results. To illustrate this, the poorer agreement between state-space and transcendental FRFs and PSD functions (in Figs. 8, 10, and 11) at the high frequencies is due to only a "fair" *s*-plane approximation for several of the SFM aerodynamic elements at reduced frequencies between 0.8 and 1.5.

Based on the convergence investigation and the two applications of the new technique, Table 2 contains a comparison of the attributes of the two forms of the dynamic load equations (where the plus and minus signs indicate whether the attribute is an advantage or a disadvantage,

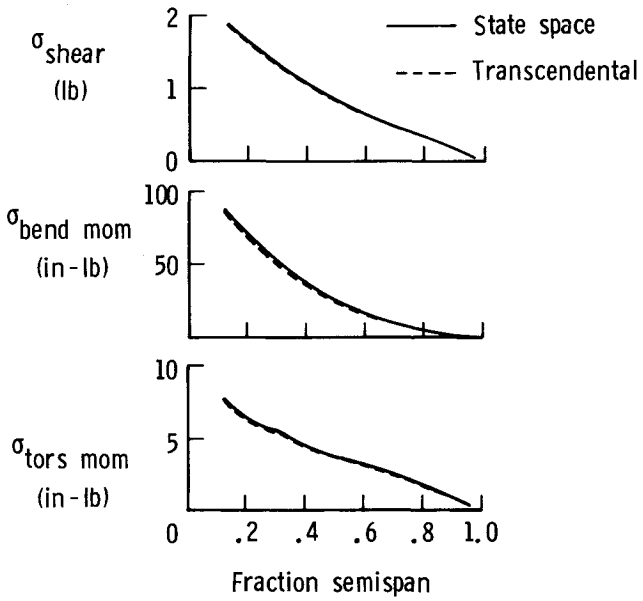

Fig. 12 Comparison of transcendental and state-space spanwise variations of dynamic load rms values.

respectively). Looking at the first two entries for each method, the major advantage of the MDM over the SFM is the former's ease of use. In contrast, the SFM has the advantage of being able to compute individual load components and, more importantly, the advantage of more rapid convergence with number of retained modes. Thus, problem size (and therefore computational core size) may be reduced with the SFM. In addition, because the SFM is now available in an LTI state-space formulation, a host of state-space computational tools may now be employed.

Conclusions

The summation-of-forces form of airplane dynamic loads equations has been expressed in an LTI state-space representation. This representation was obtained by computing a rational Laplace domain approximation of the dynamic loads. The new technique has been demonstrated by comparing dynamic loads computed the new way with those computed in a traditional frequency domain analysis where the aerodynamic forces were transcendental functions of frequency. There is excellent agreement between results obtained by the new and traditional analyses. In addition, a comparison of the summation-of-forces method (SFM) and the modal displacement method (MDM) of computing dynamic loads established that the SFM converges faster (with fewer modes) than does the MDM.

Acknowledgment

The authors wish to acknowledge the work of Charles V. Spain of Aerospace Technologies Division, PRC—Kentron, Inc. The successful completion of this study was partially due to his skillful development of the structural model of the ARW-2 cantilevered wind tunnel model.

References

[1]Sevart, F. D., "Development of Active Flutter Suppression Wind Tunnel Testing Technology," AFFDL-TR-74-126, Jan. 1975.

[2]Vepa, R., "On the Use of Pade Approximants to Represent Unsteady Aerodynamic Loads for Arbitrarily Small Motions of Wings," AIAA Paper 76-17, Jan. 1976.

[3]Edwards, J. W., "Unsteady Aerodynamic Modeling and Active Aeroelastic Control," Stanford University, Stanford, CA, Rept. SUDAAR 504, 1977 (available as NASA CR-148019).

[4]Roger, K. L., "Airplane Math Modeling Methods for Active Control Design. Structural Aspects of Active Controls," AGARD CP-228, Aug. 1977, pp. 4-1—4-11.

[5]Abel, I., "An Analytical Technique for Predicting the Characteristics of a Flexible Wing Equipped with an Active Flutter Suppression System and Comparison with Wind-Tunnel Data," NASA TP-1367, Feb. 1979.

[6]Newsom, J. R., "A Method for Obtaining Practical Flutter-Suppression Control Laws Using Results of Optimal Control Theory," NASA TP-1471, Aug. 1979.

[7]Dunn, H. J., "An Analytical Technique for Approximating Unsteady Aerodynamics in the Time Domain," NASA TP-1738, Nov. 1980.

[8]Adams, W. M. and Tiffany, S. H., "Design of a Candidate Flutter Suppression Control Law for DAST ARW-2," AIAA Paper 83-2221, Aug. 1983.

[9]Gangsaas, D. and Ly, U., "Application of a Modified Linear Quadratic Gaussian Design to Active Control of a Transport Airplane," AIAA Paper 79-1746, Aug. 1979.

[10]Mukhopadhyay, V., Newsom, J. R., and Abel, I., "A Method for Obtaining Reduced-Order Control Laws for High-Order Systems Using Optimization Techniques," NASA TP 1876, Aug. 1981.

[11]Bisplinghoff, R. L., Ashley, H., and Halfman, R. L., *Aeroelasticity*, Addison-Wesley Publishing Co., Reading, MA, 1955.

[12]Rodden, W. P., Harder, R. L., and Bellinger, E. D., "Aeroelastic Addition to NASTRAN," NASA CR-3094, March 1979.

[13]Whetstone, W. D., "EISI-EAL Engineering Analysis Language Reference Manual, System Level 209I," Engineering Information Services, Inc., San Jose, CA, July 1983.

[14]Albano, E. and Rodden, W., "A Doublet-Lattice Method for Calculating Lift Distributions on Oscillating Surfaces in Subsonic Flow," *AIAA Journal*, Vol. 7, Feb. 1969, pp. 279-285.

[15]Rowe, W. S., Winther, B. A., and Redman, M. C., "Unsteady Subsonic Aerodynamic Loadings Caused by Control Surface Motions," *Journal of Aircraft*, Vol. 11, Jan. 1974, pp. 45-54.

[16]Perry, B. III, Kroll, R. I., Miller, R. D., and Goetz, R. C., "DYLOFLEX: A Computer Program for Flexible Aircraft Flight Dynamic Loads Analyses with Active Controls," *Journal of Aircraft*, Vol. 17, April 1980, pp. 275-282.

[17]Peele, E. L. and Adams, W. M. Jr., "A Digital Program for Calculating the Interaction Between Flexible Structures, Unsteady Aerodynamics and Active Controls," NASA TM-80040, 1979.

[18]Mahesh, J. K., Stone, C. R., Garrard, W. L., and Hausman, P. D., "Active Flutter Control for Flexible Vehicles, Vol. I—Final Report," NASA CR-159160, Nov. 1979.

[19]Newsom, J. R., Adams, W. M. Jr., Mukhopadhyay, V., Tiffany, S. H., and Abel, I., "Active Controls: A Look at Analytical Methods and Associated Tools," NASA TM-86269, July 1984.